Computer Aided Design of Waveguide Devices by Mode-Matching Methods

Jorge A. Ruiz-Cruz

Escuela Politecnica Superior, Universidad Autonoma de Madrid
C/ Francisco Tomas y Valiente 11, 28049 Madrid
Spain

Jose R. Montejo-Garai and Jesus M. Rebollar

Dpto. de Electromagnetismo y Teora de Circuitos, Universidad Politecnica de Madrid
Ciudad Universitaria s/n, 28040 Madrid
Spain

1. Introduction

1.1 Waveguide devices and CAD tools

Technology is one of the key issues in the hardware design at the microwave and millimetre wave band. Its selection depends on many factors such as bandwidth, physical size, losses, power handling capability and cost. This has led to many different transmission media for implementing circuits and systems; the planar and the waveguide technologies are two representative examples.

The main advantages of planar structures are their small size and simple manufacturing. In addition, they can be easily integrated with Microwave Integrated Circuits (MIC) and Monolithic Microwave Integrated Circuits (MMIC). The microstrip transmission line is a common example of this technology, where circuits are made by printing a metallic strip on a dielectric substrate supported by a ground plane. On the other hand, waveguide devices (the type of components which will be discussed in this chapter) are constructed on metallic pipes that may have many forms. The electromagnetic waves are confined to the interior of the waveguiding structure. In contrast to planar devices, they are more cumbersome and bulkier. Their main advantage is their high power handling capabilities and high quality factor (Q), which leads to electric responses with lower insertion losses than planar technology components. In satellite applications, their robustness also becomes an advantage.

One aspect that has significantly modified the design of advanced waveguide components during the last decades has been the evolution of software modeling and Computer Aided Design (CAD) tools. Traditionally, the analysis of waveguide devices (such as couplers, filters or multiplexers) was based on approximate equivalent circuits made up of transmission lines to represent waveguiding regions and lumped elements (inductors, capacitors, transformers, resistors, etc.) to model dissipative effects and discontinuities between different transmission media. Most of the equivalent circuits for waveguide problems were developed at the MIT
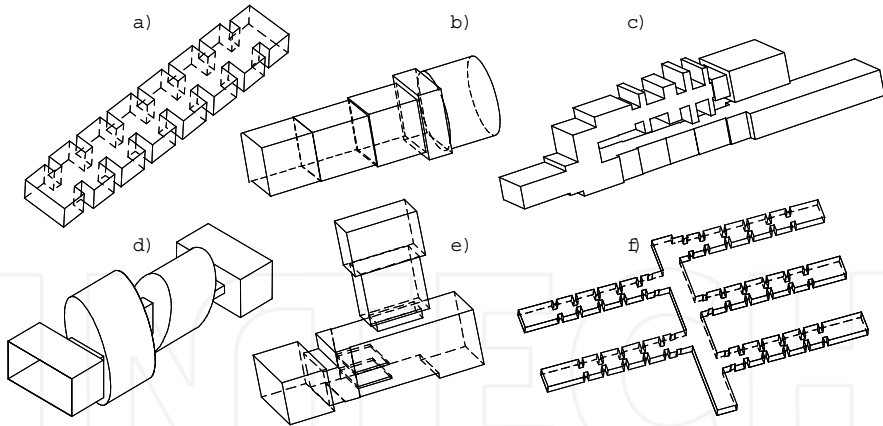
Fig. 1. Examples of waveguide devices which can be efficiently modeled by Mode-Matching: a) bandpass filter; b) square to circular waveguide transformer; c) diplexer with low-pass and high-pass filters; d) dual-Mode filter with elliptical waveguides; e) ortho-mode transducer (OMT); f) 5-channel manifold multiplexer.

Radiation Laboratory. These models, together with the advance in synthesis circuit theory, have brought about the design of many devices.

Nevertheless, the equivalent circuit approach has a number of limitations. The most significant is that equivalent circuits are only focused on modeling the fundamental mode response of the elements in the structure and the localized effect of the higher order modes. However, the interactions between the higher-order modes of the different elements and other electromagnetic effects are not taken into account. Thus, this approach leads to discrepancies between the theoretical predicted response of the device and its actual measurement. The designed prototypes following this approach hence need a relevant experimental effort and manual tuning. In a more demanding industrial sector, it seems reasonable to complement these results with other more precise methods and to evolve towards CAD tools.

New techniques to model microwave devices appear as a consequence of two facts: i) a solid comprehension of the microwave theory along with numerical methods, and ii) the development of computers. The latter allows the implementation of codes that few years ago seemed unfeasible because of their required computer resources.

There is a great variety of methods to deal with the so-called full-wave analysis of modern microwave devices (Uher et al., 1993). Among the different alternatives, two basic aspects should be addressed: i) the efficiency using the computer resources (RAM memory, disk storage and processor capabilities), and ii) the types of geometries and materials that they can handle. The methods vary from general numeric techniques (such as the Finite Element Method, Finite Differences, etc.) to quasi-analytical techniques (such as the Mode-Matching method). There also hybrid techniques combining different approaches.

Among these different CAD options, those based on Mode-Matching (MM) methods (Clarricoats & Slinn, 1966), (Drabuwitch, 1966), (Wexler, 1967) are good examples of accurate and efficient tools. The range of problems that they can tackle is more constrained in comparison with general numeric techniques. Nevertheless, when the characterization of the

device under investigation can be carried out by MM (as for instance those shown in Fig. 1), the resulting codes are very efficient and facilitate the design of components with sophisticated responses. In fact, this is the objective of this chapter: to present the main concepts of the MM techniques and to show its application to several designs for common applications.

1.2 Overview of the Mode-Matching (MM) method

The starting point for MM is to segment the problem under analysis in different waveguide regions (for instance the different rectangular waveguides in Fig. 1.a), where the total electromagnetic field is represented by the superposition of modes

$$\vec{\mathbf{E}} = \sum_n \varsigma_n^+ \vec{\mathbf{E}}_n^+ + \sum_n \varsigma_n^- \vec{\mathbf{E}}_n^- , \quad \vec{\mathbf{H}} = \sum_n \varsigma_n^+ \vec{\mathbf{H}}_n^+ + \sum_n \varsigma_n^- \vec{\mathbf{H}}_n^- . \tag{1}$$

These expansions (different for each waveguide) are constructed in order to represent any possible field inside each region. The scalar complex amplitudes $\varsigma_n^{\pm}$ are (initially) undetermined. On the other hand, the electromagnetic field of each mode $(\vec{\mathbf{E}}_n^{\pm}, \vec{\mathbf{H}}_n^{\pm})$ must be known in advance either analytically (as for the waveguides shown at App. A.5) or numerically (by means of a suitable numerical method).

The modal expansion (1) provides a formal solution to the Maxwell´s equations for each waveguide. However, for the complete resolution of the problem, the boundary conditions at the interface between the different segmented regions must be also fulfilled. A field-matching procedure is used to impose those boundary conditions, providing a relation between the amplitudes $\varsigma_n^{\pm}$ of the modes involved in all the regions. This relation is usually not simple, and requires some previous computations: the inner cross products between the modal fields.

In order to make a formal representation of the problem under investigation, the modal amplitudes in each region are usually collected in vectors. The relation of those vectors is usually expressed in terms of the Generalized Scattering Matrix (GSM). Other formulations use the Generalized Admittance or Impedance Matrix (GAM or GIM, respectively) (Conciauro et al., 1999), which are the natural option when (1) is expressed with equivalent voltages and currents instead of modal amplitudes. The term *Generalized* refers to the types of modes used in (1): propagating and evanescent modes are both required in the series to represent the field. Their amplitudes at the different regions will be related by the GSM.

As many other numerical methods, some convergence issues will appear in MM. They are related to the series in (1), which must be truncated to a finite number of modes for computational purposes. Therefore, the boundary conditions and the amplitudes obtained by MM will be an approximation whose accuracy will depend on the number of modes retained in the modal expansions. Moreover, the solution will depend not only on the number of modes used in the different regions, but also on the relation between them. This problem is known as the relative convergence problem (Mittra & Lee, 1971), (Vassallo, 1985).

These general ideas are found in the MM of very different problems. In order to see them in a more detailed form, a specific problem will be treated now: the cascade connection of different transmission systems. This is the basic structure that can be used to solve more complex problems with cubic junctions or volume-type structures with more general enclosures. The theory for the discontinuities will be developed in a unified manner, aiming to highlight the important aspects of the method not always covered in other text books. The implementation details will be given as references (as for instance the computation of the inner cross products).
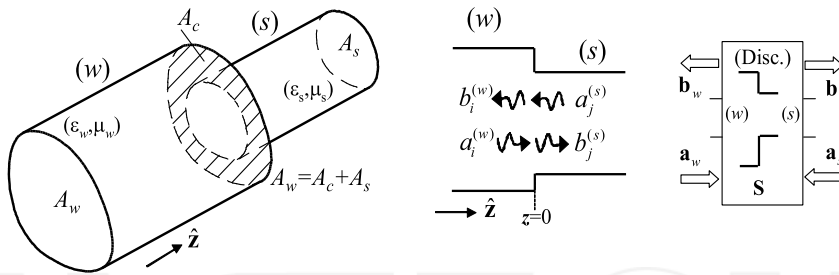
Fig. 2. Basic waveguide step with the modal amplitudes incident and scattered by the discontinuity. The Mode-Matching (MM) method provides its Generalized Scattering Matrix (GSM) as a building-block to use in more complex structures.

2. Mode-Matching method for waveguide steps

2.1 Waveguide step or discontinuity

The waveguide step or discontinuity problem arises when different transmission systems are connected in a plane transversal to the propagation direction. The type of transmission systems considered now are homogeneous cylindrical waveguides connected in the direction of their longitudinal axis z (described in App. A). The problem is detailed in Fig. 2 and it could represent, for instance, the discontinuity between two rectangular waveguides in Fig. 1.a or the discontinuity between a rectangular and a elliptical waveguide in Fig. 1.d. The goal is to have a representation of this step as a building block characterized by its GSM, which could be latter used in more complex problems.

2.2 Field-matching procedure

The electromagnetic field at both sides of the discontinuity in Fig. 2 are derived from (1). For this problem, the boundary conditions involve the fields transversal to z, evaluated at the discontinuity plane located at $z = 0$.

The transversal fields are expressed with the amplitudes of the modes incident (a) and scattered (b) by the step:

$$\vec{\mathbf{E}}_t^{(w)}\Big|_{A_w, z=0^-} = \sum_{n=1}^{N_w} (a_n^{(w)} + b_n^{(w)}) \, \vec{\mathbf{e}}_n^{(w)}, \quad \vec{\mathbf{H}}_t^{(w)}\Big|_{A_w, z=0^-} = \sum_{n=1}^{N_w} (a_n^{(w)} - b_n^{(w)}) \, \vec{\mathbf{h}}_n^{(w)} \tag{2a}$$

$$\vec{\mathbf{E}}_t^{(s)}\Big|_{A_s, z=0^+} = \sum_{m=1}^{N_s} (b_m^{(s)} + a_m^{(s)}) \, \vec{\mathbf{e}}_m^{(s)}, \quad \vec{\mathbf{H}}_t^{(s)}\Big|_{A_s, z=0^+} = \sum_{m=1}^{N_s} (b_m^{(s)} - a_m^{(s)}) \, \vec{\mathbf{h}}_m^{(s)}. \tag{2b}$$

Each term in the series[1] (already truncated to a finite number of modes N_w and N_s in each waveguide) belongs to a TEM, TE or TM mode, not necessarily propagating at the analysis frequency. The modes are orthogonal with arbitrary normalization:

$$\iint_{A_g} \vec{\mathbf{e}}_n^{(g)} \times \vec{\mathbf{h}}_m^{(g)} \cdot \hat{\mathbf{z}} \, dS = Q_n^{(g)} \delta_{nm}, \quad g \equiv w, s, \quad \delta_{nm} = 1(m=n), 0(m \neq n). \tag{3}$$

---

[1] The reversed sign for the amplitudes in the magnetic field of waveguide (s) is because the a, b modal amplitudes travel in the opoposite direction than their a, b counterpart in waveguide (w). See (30) in App. A for a more detailed description of the fields and App. A.4 for their normalization.

In this initial formulation it is considered that the cross section of waveguide (s) is completely included in the one of (w): $A_s \subseteq A_w$ (the general aperture case is studied later). The Electric and Magnetic Field Boundary Conditions (EFBC and MFBC, respectively) must be satisfied at the interface between the two waveguides:

$$
\begin{cases}
\text{EFBC in } A_w: \quad \hat{\mathbf{z}} \times \vec{\mathbf{E}}^{(w)} = \begin{cases} \mathbf{0}, & \text{in } A_c, z = 0 \\ \hat{\mathbf{z}} \times \vec{\mathbf{E}}^{(s)} & \text{in } A_s, z = 0 \end{cases} \\[4mm]
\text{MFBC in } A_s: \quad \hat{\mathbf{z}} \times \vec{\mathbf{H}}^{(w)} = \hat{\mathbf{z}} \times \vec{\mathbf{H}}^{(s)}, \quad \text{in } A_s, z = 0.
\end{cases}
\tag{4}
$$

In order to impose these boundary conditions, a *Galerkin* method is used. The first step is to test the EFBC with a generic modal magnetic field $\vec{\mathbf{h}}_j^{(w)}$ of waveguide (w). The left hand side, using (2a), leads to

$$
\iint_{A_w} (\hat{\mathbf{z}} \times \vec{\mathbf{E}}^{(w)}) \cdot \vec{\mathbf{h}}_j^{(w)} \hat{\mathbf{z}} dS = \sum_{n=1}^{N_w} (a_n^{(w)} + b_n^{(w)}) \left(\iint_{A_w} (\hat{\mathbf{z}} \times \vec{\mathbf{e}}_n^{(w)}) \cdot \vec{\mathbf{h}}_j^{(w)} \hat{\mathbf{z}} dS \right).
$$

Since the modes are orthogonal, according to (3), the previous equation becomes

$$
\iint_{A_w} (\hat{\mathbf{z}} \times \vec{\mathbf{E}}^{(w)}) \cdot \vec{\mathbf{h}}_j^{(w)} \hat{\mathbf{z}} dS = (a_j^{(w)} + b_j^{(w)}) Q_j^{(w)}.
\tag{5}
$$

Moreover, the integration in A_w can be divided in two terms, since $A_w = A_s \cup A_c$:

$$
\iint_{A_w} (\hat{\mathbf{z}} \times \vec{\mathbf{E}}^{(w)}) \cdot \vec{\mathbf{h}}_j^{(w)} \hat{\mathbf{z}} dS = \iint_{A_c} (\hat{\mathbf{z}} \times \vec{\mathbf{E}}^{(w)}) \cdot \vec{\mathbf{h}}_j^{(w)} \hat{\mathbf{z}} dS + \iint_{A_s} (\hat{\mathbf{z}} \times \vec{\mathbf{E}}^{(w)}) \cdot \vec{\mathbf{h}}_j^{(w)} \hat{\mathbf{z}} dS.
$$

Taking into account that $\hat{\mathbf{z}} \times \vec{\mathbf{E}}^{(w)} = \mathbf{0}$, in $A_c, z = 0$ and (2b), it is obtained

$$
\iint_{A_w} (\hat{\mathbf{z}} \times \vec{\mathbf{E}}^{(w)}) \cdot \vec{\mathbf{h}}_j^{(w)} \hat{\mathbf{z}} dS = \iint_{A_s} (\hat{\mathbf{z}} \times \vec{\mathbf{E}}^{(s)}) \cdot \vec{\mathbf{h}}_j^{(w)} \hat{\mathbf{z}} dS =
\tag{6}
$$

$$
= \sum_{m=1}^{N_s} (a_m^{(s)} + b_m^{(s)}) \left\{ \iint_{A_s} \vec{\mathbf{e}}_m^{(s)} \times \vec{\mathbf{h}}_j^{(w)} \cdot \hat{\mathbf{z}} dS \right\}.
$$

The integral with the modal fields is a complex number called the inner cross product X_{mj}. The process for obtaining equations (5) and (6) can be done for any $j = 1, \ldots, N_w$. The result can be expressed as

$$
Q_j^{(w)} (a_j^{(w)} + b_j^{(w)}) = \sum_{m=1}^{N_s} X_{mj} (a_m^{(s)} + b_m^{(s)}), \quad j = 1, \ldots, N_w.
\tag{7}
$$

The second step is to test the MFBC with the modal electric fields $\vec{\mathbf{e}}_i^{(w)}$ of waveguide (s). The left hand side provides an equation with the same previous type of inner cross product:

$$
\iint_{A_s} (\hat{\mathbf{z}} \times \vec{\mathbf{H}}^{(w)}) \cdot \vec{\mathbf{e}}_i^{(s)} \hat{\mathbf{z}} dS = \sum_{n=1}^{N_w} (a_n^{(w)} - b_n^{(w)}) \left\{ \iint_{A_s} \vec{\mathbf{e}}_i^{(s)} \times \vec{\mathbf{h}}_n^{(w)} \cdot \hat{\mathbf{z}} dS \right\}.
\tag{8}
$$

For the right hand side, the orthogonality of the modes in waveguide (s) is applied

$$
\iint_{A_s} (\hat{\mathbf{z}} \times \vec{\mathbf{H}}^{(w)}) \cdot \vec{\mathbf{e}}_i^{(s)} \hat{\mathbf{z}} dS = \iint_{A_s} (\hat{\mathbf{z}} \times \vec{\mathbf{H}}^{(s)}) \cdot \vec{\mathbf{e}}_i^{(s)} \hat{\mathbf{z}} dS = Q_i^{(s)} (b_i^{(s)} - a_i^{(s)}).
\tag{9}
$$

Equations (8) and (9) can be reproduced for any $i = 1, \ldots, N_s$, providing:

$$\sum_{n=1}^{N_w} X_{in}(a_n^{(w)} - b_n^{(w)}) = Q_i^{(s)}(b_i^{(s)} - a_i^{(s)}), \ i = 1, \ldots, N_s. \tag{10}$$

The resulting equations (7) and (10) are better expressed if the amplitudes are arranged in columns vectors

$$\mathbf{a}_g = \left[\cdots a_n^{(g)} \cdots \right]_{n=1,\ldots,N_g}^t, \quad \mathbf{b}_g = \left[\cdots b_n^{(g)} \cdots \right]_{n=1,\ldots,N_g}^t, \quad g \equiv w, s.$$

The normalization constants are collected in the diagonal matrices

$$\mathbf{Q}_g = \text{diag} \left[Q_n^{(g)} \right]_{n=1,\ldots,N_g}, \quad g \equiv w, s, \quad [N_g \times N_g]. \tag{11}$$

and the inner cross product in a full rectangular matrix

$$[X_{mn}] = \iint_{A_s} \vec{\mathbf{e}}_m^{(s)} \times \vec{\mathbf{h}}_n^{(w)} \cdot \hat{\mathbf{z}} dS, \quad [N_s \times N_w]. \tag{12}$$

With these definitions, the linear system obtained from the boundary conditions is expressed as

$$\begin{cases} \text{EFBC:} & \mathbf{Q}_w(\mathbf{a}_w + \mathbf{b}_w) = \mathbf{X}^t(\mathbf{a}_s + \mathbf{b}_s) & (N_w \text{ eqs.}) \\ \text{MFBC:} & \mathbf{X}(\mathbf{a}_w - \mathbf{b}_w) = \mathbf{Q}_s(\mathbf{b}_s - \mathbf{a}_s) & (N_s \text{ eqs.}) \end{cases}. \tag{13}$$

2.3 Generalized Scattering Matrix of the waveguide step

The above system (13) can be used to find the value of $\mathbf{b}_w, \mathbf{b}_s$ in terms of $\mathbf{a}_w, \mathbf{a}_s$. This relation is the Generalized Scattering Matrix (GSM) representation of the waveguide step and it can be expressed as:

$$\begin{bmatrix} \mathbf{b}_w \\ \mathbf{b}_s \end{bmatrix} = \begin{bmatrix} \mathbf{S}_{ww} & \mathbf{S}_{ws} \\ \mathbf{S}_{sw} & \mathbf{S}_{ss} \end{bmatrix} \begin{bmatrix} \mathbf{a}_w \\ \mathbf{a}_s \end{bmatrix}, \mathbf{b} = \mathbf{S}\mathbf{a}.$$

The terms of the GSM, once (13) is used, are:

$$\mathbf{S} = \begin{bmatrix} \mathbf{Q}_w^{-1}\mathbf{X}^t\mathbf{F}\mathbf{X} - \mathbf{I}_w & \mathbf{Q}_w^{-1}\mathbf{X}^t\mathbf{F}\mathbf{Q}_s \\ \mathbf{F}\mathbf{X} & \mathbf{F}\mathbf{Q}_s - \mathbf{I}_s \end{bmatrix}, \quad \mathbf{F} = 2(\mathbf{Q}_s + \mathbf{X}\mathbf{Q}_w^{-1}\mathbf{X}^t)^{-1}, \tag{14}$$

where $\mathbf{I}_g$ is the identity matrix of size N_g. Therefore, in conclusion, for obtaining the GSM is only required to select a set of modes in each waveguide, to fill the normalization and inner cross product matrices (discussed below) and to perform the previous matrix operations.

The question to address now is the effect of varying the number of selected modes on the solution of the problem. In addition, since different modal series are involved, the solution also depends on the relative truncation criterion for N_w/N_s. This problem occurs in any MM approach and is called the relative convergence problem (Leroy, 1983), (Itoh (editor), 1989, Ch. 9 and 11).

The issue to highlight is that the convergence depends not only on the number of modes, but also in the relation between the numbers used in the different expansions. If the relation is not

appropriate, the results may not converge even increasing the number of modes. It has been shown that the optimum mode selection for a bifurcation in parallel-plate waveguide (Mittra & Lee, 1971) is a number of modes proportional to the aspect ratio of each waveguide cross section. The key idea is that the different expansions must reach the same maximum spatial resolution.

In practice, this result is generalized for other discontinuities and a usual criterion is to select the mode ratio the same as the aspect ratio. However, this is a starting point and does not guarantee the convergence. Other similar criterion is to take into account all the modes in the waveguides whose cutoff wavenumbers are lower than a certain $k_{c,max}$. Then, the convergence is checked looking at the results when $k_{c,max}$ is increased.
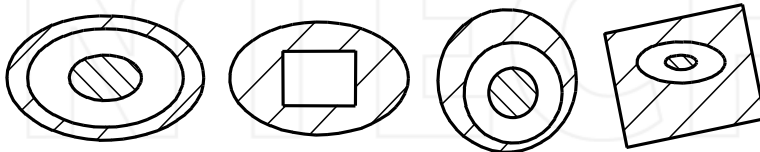

Fig. 3. Examples of cross-sections in discontinuities involving canonical waveguides (rectangular, circular, elliptical, coaxial).

2.4 Inner cross products between the modal fields

The computation of the inner cross products is better addressed if they are factorized as follows. They can be divided into a geometry factor (the normalized inner cross products) and the frequency and waveguide medium information (the modal wave impedances/admittances and, maybe, the normalization Q). According to the expressions for the modal fields in App. A (equations (33),(36),(39)), the inner products can be factorized as follows

$$X_{mn} = \iint_{A_s} \vec{\mathbf{e}}_m^{(s)} \times \vec{\mathbf{h}}_n^{(w)} \cdot \hat{\mathbf{z}} dS = \{ (Q_m^{(s)})^{\frac{1}{2}} (Z_m^{(s)})^{\frac{1}{2}} \} \bar{X}_{mn} \{ (Y_n^{(w)})^{\frac{1}{2}} (Q_n^{(w)})^{\frac{1}{2}} \}. \tag{15}$$

The terms $\bar{X}_{mn}$ (the normalized inner cross products) are real numbers independent of frequency and the waveguide media and exclusively dependent on the geometry of the discontinuity, since they only involve the real functions defined in App. A:

$$\bar{X}_{mn} = \iint_{A_s} \vec{\mathbf{\Phi}}_{Em}^{(s)} \times \vec{\mathbf{\Phi}}_{Hn}^{(w)} \cdot \hat{\mathbf{z}} dS = \iint_{A_s} \vec{\mathbf{\Phi}}_{Em}^{(s)} \cdot \vec{\mathbf{\Phi}}_{En}^{(w)} dS = \iint_{A_s} \vec{\mathbf{\Phi}}_{Hm}^{(s)} \cdot \vec{\mathbf{\Phi}}_{Hn}^{(w)} dS. \tag{16}$$

Thus, in a frequency sweep, they can be computed once and be multiplied by diagonal matrices to update the GSM expression (14) at any frequency point:

$$\mathbf{X} = \{ \mathbf{Q}_s^{\frac{1}{2}} \mathbf{Z}_s^{\frac{1}{2}} \} \bar{\mathbf{X}} \{ \mathbf{Y}_w^{\frac{1}{2}} \mathbf{Q}_w^{\frac{1}{2}} \}. \tag{17}$$

To simplify the notation, $\bar{X}_{sw}$ is used now (instead of $\bar{X}_{mn}$) for an inner product between a mode of the smaller waveguide obtained from Φ_s and one of the larger derived from Φ_w. There are two equivalent approaches (shown in Table 1) to calculate $\bar{X}_{sw}$: the surface integral formulation obtained from the definition and the contour integral formulation derived later in (Figlia & Gentili, 2002), (Bozzi et al., 2002). In addition, it can be shown that there are some

$\bar{X}_{sw}$	TEM_w	TE_w	TM_w
TEM_s	$\iint\limits_{A_s} \nabla_t \Phi_w \cdot \nabla_t \Phi_s dS$	0	$\iint\limits_{A_s} \nabla_t \Phi_w \cdot \nabla_t \Phi_s dS$
TE_s	$\iint\limits_{A_s} \nabla_t \Phi_w \times \nabla_t \Phi_s \cdot \hat{\mathbf{z}} dS$	$\iint\limits_{A_s} \nabla_t \Phi_w \cdot \nabla_t \Phi_s dS$	$\iint\limits_{A_s} \nabla_t \Phi_w \times \nabla_t \Phi_s \cdot \hat{\mathbf{z}} dS$
TM_s	0	0	$\iint\limits_{A_s} \nabla_t \Phi_w \cdot \nabla_t \Phi_s dS$

$$\bar{X}_{sw} = \iint_{A_s} \vec{\boldsymbol{\Phi}}_{Es} \times \vec{\boldsymbol{\Phi}}_{Hw} \cdot \hat{\mathbf{z}} dS$$

(s)-(w)	$\bar{X}_{sw}$
TEM-TEM	$\oint\limits_{C_s} \Phi_w \nabla_t \Phi_s \cdot \hat{\mathbf{n}}_s dl = \oint\limits_{C_s} \Phi_s \nabla_t \Phi_w \cdot \hat{\mathbf{n}}_s dl$
TEM-TM	$\oint\limits_{C_s} \Phi_w \nabla_t \Phi_s \cdot \hat{\mathbf{n}}_s dl$
TE-TEM	$\oint\limits_{C_s} \Phi_w \nabla_t \Phi_s \cdot (\hat{\mathbf{z}} \times \hat{\mathbf{n}}_s) dl = -\oint\limits_{C_s} \Phi_s \nabla_t \Phi_w \cdot (\hat{\mathbf{z}} \times \hat{\mathbf{n}}_s) dl$
TE-TM	$\oint\limits_{C_s} \Phi_w \nabla_t \Phi_s \cdot (\hat{\mathbf{z}} \times \hat{\mathbf{n}}_s) dl = -\oint\limits_{C_s} \Phi_s \nabla_t \Phi_w \cdot (\hat{\mathbf{z}} \times \hat{\mathbf{n}}_s) dl$
TE-TE	$\frac{k_{cs}^2}{k_{cs}^2 - k_{cw}^2} \oint_{C_s} \Phi_s \nabla_t \Phi_w \cdot \hat{\mathbf{n}}_s dl \qquad\qquad k_{cs} \neq k_{cw}$ $\frac{-1}{2} \oint\limits_{C_s} \Phi_s \nabla_t (\rho_{ar} \frac{\partial \Phi_w}{\partial \rho_{ar}}) \cdot \hat{\mathbf{n}}_s dl = \frac{-k_{cw}}{2} \oint\limits_{C_s} \Phi_s \frac{\partial (\nabla_t \Phi_w \cdot \hat{\mathbf{n}}_s)}{\partial k_{cw}} dl \quad k_{cs} = k_{cw}$
TM-TM	$\frac{k_{cw}^2}{k_{cw}^2 - k_{cs}^2} \oint\limits_{C_s} \Phi_w \nabla_t \Phi_s \cdot \hat{\mathbf{n}}_s dl \qquad\qquad k_{cs} \neq k_{cw}$ $\frac{1}{2} \oint\limits_{C_s} \rho_{ar} \frac{\partial \Phi_w}{\partial \rho_{ar}} \nabla_t \Phi_s \cdot \hat{\mathbf{n}}_s dl = \frac{k_{cw}}{2} \oint\limits_{C_s} \frac{\partial \Phi_w}{\partial k_{cw}} \nabla_t \Phi_s \cdot \hat{\mathbf{n}}_s dl \quad k_{cs} = k_{cw}$

Table 1. Normalized inner cross products: surface and contour integral formulations (Figlia & Gentili, 2002), (Bozzi et al., 2002). ($C_s = \delta A_s$ is the contour of A_s.)

type of inner cross products that are always zero (Gentili, 1991). These cases are included in the same Table 1.

The computation of the integrals in $\bar{X}_{sw}$ for a discontinuity between two rectangular waveguides can be done analytically leading to very compact expressions (in fact, this problem was one of the basis for the developing of MM (Patzelt & Arndt, 1982)). However, this is not always the case, since the modal functions can be obtained by means of other numerical methods. If a numerical evaluation of the integrals is required, the contour integral formulation provides the most efficient approach, although it is more sensitive to numerical errors than the surface integral version.

Moreover, even when the TEM, TE and TM solutions Φ_s, Φ_w are available with closed expressions (see App. A.5) the integrals may not be direct and must involve a careful study. Some discontinuity cross-sections are shown in Fig. 3 and a fast computation of $\bar{X}_{sw}$ may involve transformations among plane, circular and elliptical waves. Some examples are found in (Orfanidis et al., 2000), (Zhongxiang & MacPhie, 1995), (MacPhie & Wu, 1995), (Mongiardo & Tomassoni, 2000), (Chan & Judah, 1997).

2.5 Properties of the GSM obtained by MM

The formal properties that must satisfy the GSM (including evanescent modes) of a waveguide junction (not only for a waveguide step) can be shown by applying the classic electromagnetic theorems of Lorentz, Poynting and Self-Reaction (Haskal, 1964).

The properties are investigated now in the context of the MM formulations (Omar et al., 1994). The matter to discern is when these properties give any information about how the electromagnetic problem is being solved.

The properties will be related to the normalization of the modes. For instance, the GSM in (14) is Q-symmetric ($\mathbf{QS} = \mathbf{S}^t\mathbf{Q}$) and self-inverting ($\mathbf{S} = \mathbf{S}^{-1}$ or $\mathbf{SS} = \mathbf{I}$). This is shown exclusively by means of algebraic operations, beginning with (14) and using $\mathbf{XQ}_w^{-1}\mathbf{X}^t = 2\mathbf{F}^{-1} - \mathbf{Q}_s$. Therefore, these properties hold regardless of the number of modes retained in the field expansions and the value (whether calculated correctly or not) of the inner products.

An alternative derivation of these properties is based on showing that equations (13) impose the same type of relations that the Lorentz and Self-Reaction theorems. This approach is now followed for the Poynting theorem. The proof requires to use the diagonal matrices containing the complex power carried by each mode in each waveguide (g) of the discontinuity

$$\mathbf{P}_g = \mathrm{diag}\left[P_n^{(g)}\right]_{n=1,\dots,N_g}, \quad P_n^{(g)} = \iint_{A_g} \vec{\mathbf{e}}_n^{(g)} \times \vec{\mathbf{h}}_n^{(g)*} \cdot \hat{\mathbf{z}}dS.$$

In addition, the modal amplitudes and the matrices are arranged in matrix form, as for instance to express the relation (43) shown in the App. A.4 between $\mathbf{P}$ and $\mathbf{Q}$

$$\mathbf{P} = \mathbf{Z}^{\frac{1}{2}}(\mathbf{Y}^{\frac{1}{2}})^{\dagger}\mathbf{Q}^{\frac{1}{2}}(\mathbf{Q}^{\frac{1}{2}})^{\dagger}, \tag{18}$$

where † is the transpose and conjugate matrix operation. A further block division, exclusive for lossless ports, classifies the modes in propagating (p) and evanescent (v), regardless of its physical port:

$$\mathbf{S} = \begin{bmatrix} \mathbf{S}_{pp} & \mathbf{S}_{pv} \\ \mathbf{S}_{vp} & \mathbf{S}_{vv} \end{bmatrix}, \quad \mathbf{P} = \begin{bmatrix} \mathbf{P}_p & 0 \\ 0 & \mathbf{P}_v \end{bmatrix}, \quad \mathbf{Q} = \begin{bmatrix} \mathbf{Q}_p & 0 \\ 0 & \mathbf{Q}_v \end{bmatrix}.$$

The $\mathbf{S}_{pp}$ matrix is what is usually understood by the S-parameters of the device, and it is extracted from the GSM just taking the parameters relating propagating modes. These are the parameters (in dB) that are plotted later in Sec. 4.

The Poynting theorem is related to the complex power flowing into $+\hat{\mathbf{z}}$ at port w:

$$\Omega_{A_w} = \frac{1}{2}\iint_{A_w} \vec{\mathbf{E}}^{(w)} \times \vec{\mathbf{H}}^{(w)*} \cdot \hat{\mathbf{z}}dS = \frac{1}{2}(\mathbf{a}_w - \mathbf{b}_w)^{\dagger}\mathbf{P}_w(\mathbf{a}_w + \mathbf{b}_w). \tag{19}$$

A similar expression would hold for port s. Now, Ω_{A_w} is transformed by (13) along with the following relation

$$\mathbf{P}_w\mathbf{Q}_w^{-1}\mathbf{X}^t = (\mathbf{P}_s^{\dagger}\mathbf{Q}_s^{-1}\mathbf{X})^{\dagger}. \tag{20}$$

This last expression comes from the $\mathbf{P}$ and $\mathbf{Q}$ relation (18) and the $\mathbf{X}$ factorization (17). As a result, it can be shown that $\Omega_{A_w} = \Omega_{A_s}$, i.e., the complex power flow is conserved when using (13).

This is the relation that the Poynting theorem states for this particular junction. Hence, the results from (Haskal, 1964) could be applied here. Particularly, if the ports are lossless, $\mathbf{S}_{pp}$
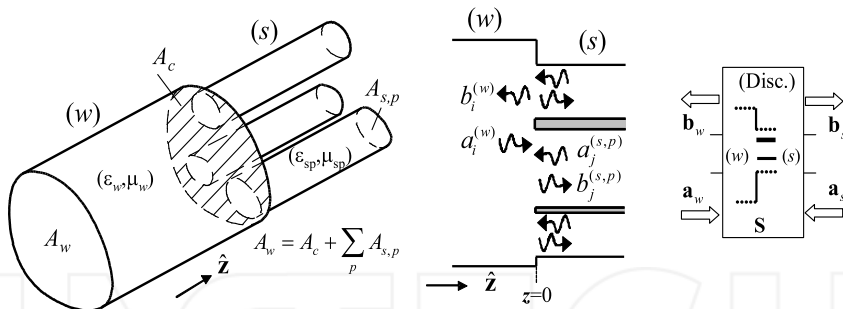
Fig. 4. Waveguide step with one main waveguide (w) and P smaller waveguides. This the multiport case (or P-furcation) whose GSM is also obtained by MM.

is P_p-unitary ($\mathbf{P}_p \mathbf{S}_{pp}^{-1} = \mathbf{S}_{pp}^\dagger \mathbf{P}_p$). This yields the familiar unitary property $\mathbf{S}_{pp}^{-1} = \mathbf{S}_{pp}^\dagger$ under a normalization with $\mathbf{P}_p = |\mathbf{Q}_p| = \mathbf{I}$.

This last result relies exclusively on the form of the linear system (13) and (20). If the real matrix $\bar{\mathbf{X}}$ is wrong and $\mathbf{X}$ is generated by (17), the P_p-unitary property continues being satisfied.

In conclusion, the GSM in (14) is self-inverting ($\mathbf{S} = \mathbf{S}^{-1}$). Upon the common modal normalization $\mathbf{Q} = \mathbf{I}$, the GSM is symmetric ($\mathbf{S} = \mathbf{S}^t$) and, for lossless ports, $\mathbf{S}_{pp}$ is unitary ($\mathbf{S}_{pp}^{-1} = \mathbf{S}_{pp}^\dagger$). These properties are satisfied exclusively by the form of the equations to be solved, without any relation to the boundary condition fulfillment. They are guaranteed by how the GSM is constructed, and they do not give any information about how the electromagnetic problem is being solved.

3. Extension to other type of steps and cascading

3.1 Extension to the multiport case: P-furcation

The formulation can be easily extended to the multiport case in Fig. 4, provided that the inner product matrix is constructed in blocks corresponding to the subregions:

$$\mathbf{X} = \left[\cdots \mathbf{X}^{(p)t} \cdots \right]_{p=1,\ldots,P}^t, \quad \left[\sum_{p=1}^{P} N_{s,p} \times N_w \right]. \tag{21}$$

The block matrices $\mathbf{X}^{(p)}$ are defined like (12) and contain the inner products between the electric modal fields in waveguide (s, p) and the magnetic modal fields in waveguide (w), integrating in the surface of the smaller waveguide $A_{s,p}$. In this problem, the multiport (s) collects the $N_{s,p}$ amplitudes of all the different modal series in each waveguide (s, p).

3.2 Extension to consider the losses at the discontinuity wall

An extension of the above formulation is proposed in (Shen & MacPhie, 1990) to evaluate the effect of the losses produced by real conductors in the steps of Figs. 2 and 4. The field-matching procedure relies on assuming a surface impedance boundary condition (Leontovich condition (Senior, 1960)) at the wall A_c:
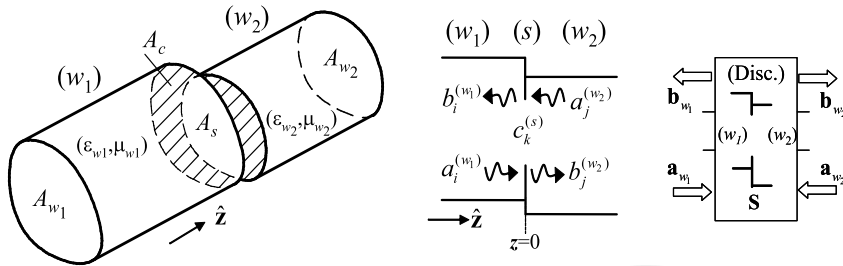
Fig. 5. Waveguide discontinuity with general aperture step (compare with Fig. 2).

$$
\begin{cases}
\text{EFBC in } A_w\text{:} \quad \hat{\mathbf{z}} \times \vec{\mathbf{E}}^{(w)} =
\begin{cases}
Z_c(\vec{\mathbf{H}}^{(w)} \times \hat{\mathbf{z}}), & \text{in } A_c, z = 0 \\
\hat{\mathbf{z}} \times \vec{\mathbf{E}}^{(s)} & \text{in } A_s, z = 0
\end{cases} \\
\text{MFBC in } A_s\text{:} \quad \hat{\mathbf{z}} \times \vec{\mathbf{H}}^{(w)} = \hat{\mathbf{z}} \times \vec{\mathbf{H}}^{(s)}, \quad \text{in } A_s, z = 0
\end{cases}
$$

with surface impedance, assuming good conductor, given by:

$$
Z_c = Y_c^{-1} = \frac{(1+j)}{\sigma\delta} = (1+j)\sqrt{\frac{\pi f \mu}{\sigma}}. \tag{22}
$$

The boundary conditions are imposed by means of a *Galerkin* method, providing:

$$
\begin{cases}
\text{EFBC:} \quad \mathbf{Q}_w(\mathbf{a}_w + \mathbf{b}_w) = \mathbf{X}^t(\mathbf{a}_s + \mathbf{b}_s) + \mathbf{L}_c(\mathbf{a}_w - \mathbf{b}_w) & (N_w \text{ eqs.}) \\
\text{MFBC:} \quad \mathbf{X}(\mathbf{a}_w - \mathbf{b}_w) = \mathbf{Q}_s(\mathbf{b}_s - \mathbf{a}_s) & (N_s \text{ eqs.}).
\end{cases} \tag{23}
$$

The resolution of this linear system yields the GSM of the step in the following form:

$$
\mathbf{S} = \begin{bmatrix} \mathbf{I} - \mathbf{F}\mathbf{Q}_w & \mathbf{F}\mathbf{X}^t \\ \mathbf{Q}_s^{-1}\mathbf{X}\mathbf{F}\mathbf{Q}_w & \mathbf{I} - \mathbf{Q}_s^{-1}\mathbf{X}\mathbf{F}\mathbf{X}^t \end{bmatrix}, \quad \mathbf{F} = 2(\mathbf{Q}_w + \mathbf{X}^t\mathbf{Q}_s^{-1}\mathbf{X} + \mathbf{L}_c)^{-1}. \tag{24}
$$

The inner products in $\mathbf{X}$ remains as (12) and, in the multiport case, are constructed in blocks as (21). The new inner products are expressed as

$$
[L_{c,mn}] = Z_c \iint_{A_c} \vec{\mathbf{h}}_m^{(w)} \cdot \vec{\mathbf{h}}_n^{(w)} dS, \quad [N_w \times N_w], \tag{25}
$$

and are calculated by integrating the modes of the larger waveguide on the conductor wall. Coherently, when the conductivity is infinite, $\mathbf{L}_c$ is null and (24) becomes (14).

3.3 Extension for the general aperture case

This section presents another type of step shown in Fig. 5, whose main feature is that the aperture at the discontinuity does not coincide with any of the input/output waveguide cross

sections. In this case, a new electric field expansion is made at the aperture surface $A_s \subseteq A_{w_1}, A_{w_2}$, expressing the boundary conditions as:

$$\vec{\mathbf{E}}^{(s)}\bigg|_{A_s, z=0} = \sum_{k=1}^{N_s} c_k^{(s)} \vec{\mathbf{e}}_k^{(s)}, \begin{cases} \text{EFBC in } A_g: & \hat{\mathbf{z}} \times \vec{\mathbf{E}}^{(g)} = \begin{cases} 0, & \text{in } A_c, z=0 \\ \hat{\mathbf{z}} \times \vec{\mathbf{E}}^{(s)} & \text{in } A_s, z=0 \end{cases} \\ \text{MFBC in } A_s: & \hat{\mathbf{z}} \times \vec{\mathbf{H}}^{(w_1)} = \hat{\mathbf{z}} \times \vec{\mathbf{H}}^{(w_2)}, \text{ in } A_s, z=0. \end{cases}$$

The two EFBC's (in A_{w_1}, A_{w_2}) are tested by the magnetic modal fields in (w_1) and (w_2), respectively, providing $N_{w1} + N_{w2}$ equations. The MFBC is tested by $\vec{\mathbf{e}}_k^{(s)}$ (the modal electric fields of the expansion at A_s), resulting in N_s equations. This leads to the following linear system with new inner products X:

$$\begin{cases} \text{EFBC:} & \mathbf{Q}_{w_1}(\mathbf{a}_{w_1} + \mathbf{b}_{w_1}) = \mathbf{X}_{w_1}^t \mathbf{c}_s, \quad \mathbf{Q}_{w_2}(\mathbf{a}_{w_2} + \mathbf{b}_{w_2}) = \mathbf{X}_{w_2}^t \mathbf{c}_s \\ \text{MFBC:} & \mathbf{X}_{w_1}(\mathbf{a}_{w_1} - \mathbf{b}_{w_1}) = \mathbf{X}_{w_2}(\mathbf{b}_{w_2} - \mathbf{a}_{w_2}) \end{cases}, \tag{26}$$

$$[X_{g,mn}] = \iint_{A_s} \vec{\mathbf{e}}_m^{(s)} \times \vec{\mathbf{h}}_n^{(g)} \cdot \hat{\mathbf{z}} dS, \quad g \equiv w_1, w_2, \quad [N_s \times N_g].$$

This system is solved for the GSM of the general aperture step:

$$\mathbf{S} = \begin{bmatrix} \mathbf{Q}_{w_1}^{-1}\mathbf{X}_{w_1}^t \mathbf{F}\mathbf{X}_{w_1} - \mathbf{I}_{w_1} & \mathbf{Q}_{w_1}^{-1}\mathbf{X}_{w_1}^t \mathbf{F}\mathbf{X}_{w_2} \\ \mathbf{Q}_{w_2}^{-1}\mathbf{X}_{w_2}^t \mathbf{F}\mathbf{X}_{w_1} & \mathbf{Q}_{w_2}^{-1}\mathbf{X}_{w_2}^t \mathbf{F}\mathbf{X}_{w_2} - \mathbf{I}_{w_2} \end{bmatrix} \tag{27}$$

with $\mathbf{F} = 2(\mathbf{X}_{w_1}\mathbf{Q}_{w_1}^{-1}\mathbf{X}_{w_1}^t + \mathbf{X}_{w_2}\mathbf{Q}_{w_2}^{-1}\mathbf{X}_{w_2}^t)^{-1}$.
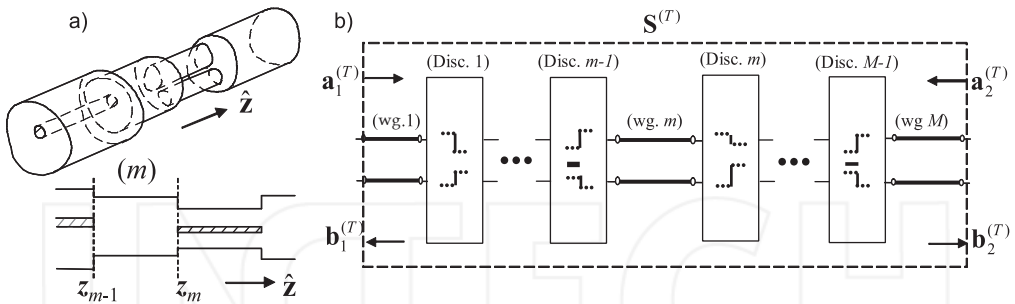

Fig. 6. a) Several waveguides with different cross section cascaded in the longitudinal direction, with its segmentation scheme in $\hat{\mathbf{z}}$; b) Cascading of GSMs. Each one could represent a waveguide step (or any other building-block in other structures).

3.4 Cascading of waveguide discontinuities

The overall characterization of a structure made up of a number of discontinuities as in Fig. 6.a is obtained by cascading the individual GSMs, using simple matrix operations. The building-blocks for the structure in Fig. 6.a belong to the waveguide steps shown in previous sections, providing the block scheme shown in Fig. 6.b.

Consider two consecutive blocks (A) and (B) in Fig. 6.b (they could be for instance the discontinuities m and $m-1$). Each block is characterized by its own GSM: $\mathbf{b}^{(A)} = \mathbf{S}^{(A)}\mathbf{a}^{(A)}$ and $\mathbf{b}^{(B)} = \mathbf{S}^{(B)}\mathbf{a}^{(B)}$. Both blocks are connected by a waveguide (which could have multiple regions) of length l, where N_{AB} modes are considered. Since the modal amplitudes vary with with $e^{-\gamma_n l}$ (see (30)), the vectors with the modal amplitudes at that region are related by:

$$\mathbf{a}_1^{(B)} = \mathbf{Y}\mathbf{b}_2^{(A)}, \ \ \mathbf{a}_2^{(A)} = \mathbf{Y}\mathbf{b}_1^{(B)}, \ \ \mathbf{Y} = \mathrm{diag}[e^{-\gamma_n l}]_{n=1,\ldots N_{AB}}. \tag{28}$$

It is implicitly considered that $\mathbf{S}^{(A)}$ and $\mathbf{S}^{(B)}$ have computed with $N_{AB} = N_2^{(A)} = N_1^{(B)}$. After the required algebra, the new GSM $\mathbf{b}^{(C)} = \mathbf{S}^{(C)}\mathbf{a}^{(C)}$ representing the whole composite block is given by:

$$\mathbf{S}^{(C)} = \begin{bmatrix} \mathbf{S}_{11}^{(A)} + \mathbf{S}_{12}^{(A)}\mathbf{Y}\mathbf{H}\mathbf{S}_{11}^{(B)}\mathbf{Y}\mathbf{S}_{21}^{(A)} & \mathbf{S}_{12}^{(A)}\mathbf{Y}\mathbf{H}\mathbf{S}_{12}^{(B)} \\ \mathbf{S}_{21}^{(B)}\mathbf{Y}(\mathbf{I}_{AB} + \mathbf{S}_{22}^{(A)}\mathbf{Y}\mathbf{H}\mathbf{S}_{11}^{(B)}\mathbf{Y})\mathbf{S}_{21}^{(A)} & \mathbf{S}_{22}^{(B)} + \mathbf{S}_{21}^{(B)}\mathbf{Y}\mathbf{S}_{22}^{(A)}\mathbf{Y}\mathbf{H}\mathbf{S}_{12}^{(B)} \end{bmatrix},$$

$$\mathbf{H} = (\mathbf{I}_{AB} - \mathbf{S}_{11}^{(B)}\mathbf{Y}\mathbf{S}_{22}^{(A)}\mathbf{Y})^{-1}, \quad [N_{AB}, N_{AB}]. \tag{29}$$

This process can be repeated iteratively till the overall GSM representing the total structure (T) in Fig. 6.b is obtained. This procedure is not only found in the context of the Mode-Matching method. It can be applied to many other problems, where the structure is segmented in blocks. The GSM of those blocks is obtained by any suitable method and the whole response is obtained by cascading.

4. Analysis and design of waveguide devices

4.1 Design approach

The previous sections have been focused on the analysis part of the CAD for waveguide devices. This part has to be complemented with a design approach, which is outlined now. Fig. 7 illustrates the typical flow chart used in many microwave devices. From the given specifications, a circuit model (if available) is obtained to lead the synthesis of the waveguide structure. Next, an initial set of physical dimensions are determined based on simple circuits and/or simplified models. Once the complete physical model is generated, a MM simulation is performed to obtain the S-parameters of the structure.

This preliminary response of the device using the initial dimensions will usually be relatively poor, since the original design did not take into account the higher-order mode interactions among the different parts of the structure. Then, the simulated response is compared with the circuit model response, and an error or cost function is computed. Using an optimization routine, the dimensions of the device are adjusted to minimize the cost function (see Fig. 7). This process is repeated until the desired response is achieved. This approach has been followed for the structures introduced in the next subsections.

4.2 H-plane bandpass filter in rectangular waveguide

An H-plane filter (see Fig. 8.a) is used to illustrate the different MM formulations shown above. The filter is analyzed considering that the conductor walls are not perfect in order to evaluate the insertion loss produced by real conductors (Ruiz-Cruz et al., 2002). This subject is an important engineering task, especially for passive components in satellite communication systems.
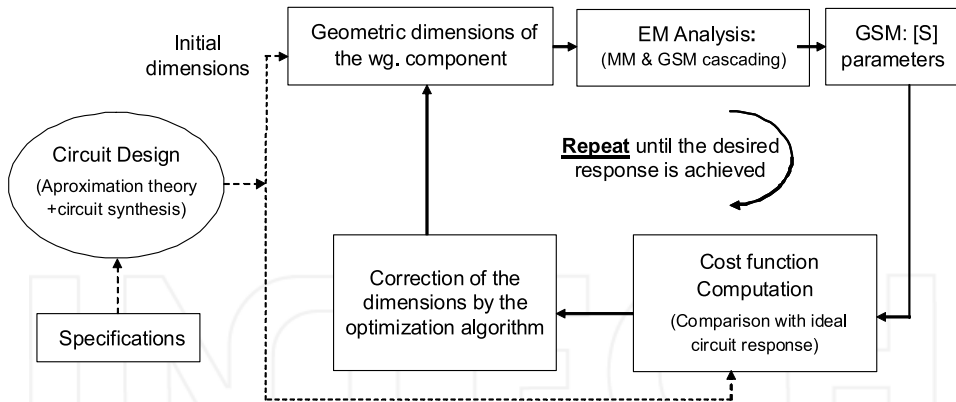
Fig. 7. Optimization cycle for designing a waveguide component.

Starting with the ideal case ($\sigma = \infty$), the different discontinuities are computed by formulation in Subsec. 2.2 and cascaded together to get the filter response. However, for the case $\sigma \neq \infty$, two models are used: i) the formulation in Subsec. 3.2, using the Leontovich condition at walls A_c (Fig. 8.b) and ii) the use of a trifurcation with lossy waveguides (Fig. 8.c). This last model simulates the solid conductors by imaginary waveguides filled with a lossy dielectric. The resultant trifurcation problem is solved as in Subsec. 3.1.

Both models take into account the losses at the lateral waveguide walls by means of modifying the propagation constant of the propagating modes (Collin, 1991), adding an attenuation constant α_c owing to the finite metal conductivity: $\gamma|_{\sigma \neq \infty} \approx \alpha_c + \gamma|_{\sigma = \infty}$. This is a common approximation for good conductors.

The results of a pass-band Chebychev filter, with 2.4% relative bandwidth in Ku frequency band, are shown in Fig. 8.d. The designed sixth order filter is implemented by means of symmetric inductive irises in WR75 waveguide. The responses that are being compared in Fig. 8.d correspond to the measurements and the simulations in the ideal and lossy cases. As expected, the three return loss responses are similar for good conductors (the simulations used $\sigma = 4.8 \cdot 10^7 S/m$).

Fig. 8.e shows the detail for the insertion loss for the Leontovich, trifurcation, FEM (HFSS, available at www.ansoft.com), circuit models and the measured results. The circuit model consists on the classic impedance inverters connected by $\lambda_g/2$ transmission lines, using the approximation for the propagation constant $\gamma|_{\sigma \neq \infty}$. It is seen that the trifurcation approach yields values slightly under the predicted by the Leontovich model. However, the agreement among the different procedures for the insertion loss and the experimental results is satisfactory.

4.3 Coaxial probe and stripline bifurcation

Other interesting problem that can been analyzed by MM is a coaxial probe inside a rectangular waveguide, shown in the inset of Fig. 9.a. From a CAD point of view, this structure can be represented as the cascade of uniform waveguides with different cross sections and, then, suitable for being solved by MM.
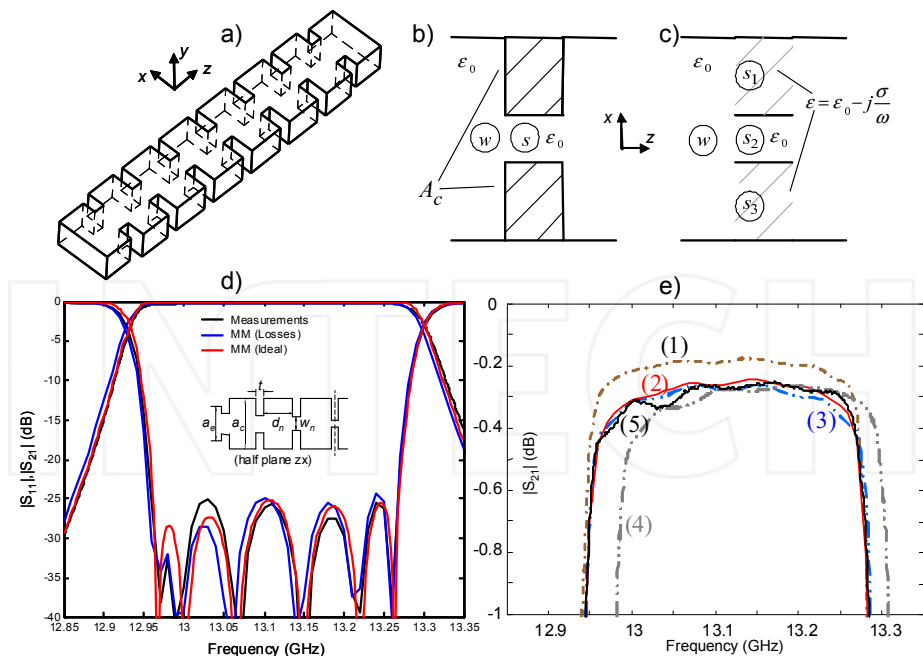
Fig. 8. a) Rectangular waveguide *H*-plane filter; b) Leontovich model: the cavity-iris disconti-nuity takes into account non perfect conductor boundary conditions at the wall A_c; c) Trifur-cation model: the non perfect conductor is replaced by a virtual rectangular waveguide with lossy dielectric. d) Return and insertion loss. e) Detail of the insertion loss: 1-trifurcation model, 2-Leontovich formulation, 3-circuit model, 4-HFSS, 5-measurements. Dimensions (mm): $a_e = 19.05$, $b_e = 9.525$, $a_c = 21.9$, $t = 3.75$, $d_{1-3} = 10.51$, 11.95, 12.13, $w_{1-4} = 9.73$, 6.68, 6.11, 6.03.

In this scope, the modes of the waveguide in the probe region can be calculated in different ways. The model followed here (Ruiz-Cruz et al., 2004) consists of a generalized stripline whose inner conductor has a stepped profile in order to approximate the desired cross section of the probe. Depending on the application, the probe can have a different size than the inner conductor of the coaxial line, but it is usually very thin. Therefore, two or three steps, even one (*i.e.* square) in some cases, give accurate results. This is shown not just in one isolated discontinuity but in the response of the cascading of several waveguide steps.

The basic discontinuity to be modeled is made up of a coaxial waveguide and the general-ized stripline. Other discontinuities involved in the problem are between ridge waveguides and rectangular waveguides. The modes of these waveguides have been computed using the Generalized Transverse Resonance (GTR) (Itoh (editor), 1989), but other techniques are also possible.

The coaxial-to-rectangular waveguide transition designed and measured in (Gerini & Guglielmi, 2001) is calculated in Fig. 9.a. In the structure, the inner conduc-tor of the SMA connector is extended to contact a ridge waveguide section. The MM response
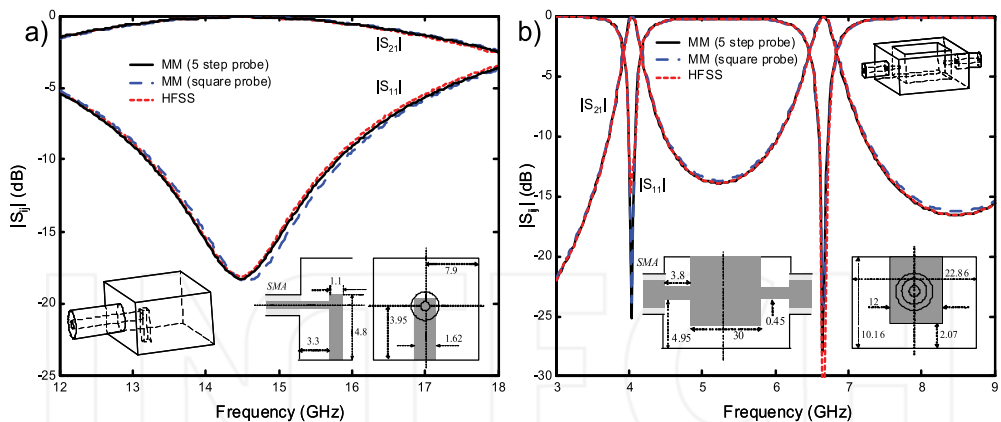
Fig. 9. a) Coaxial (50Ω SMA) to rectangular waveguide transition of (Gerini & Guglielmi, 2001). b) Back-to-back coaxial (50Ω SMA) to ridge waveguide junction. SMA dimensions (mm): $r_{in} = 0.645$, $r_{ex} = 2.045$, $\varepsilon_r = 1.97$.

is compared with the HFSS, showing good agreement but with much less computation time (as in the other examples).

To see the effect of the number of sections in the generalized stripline, the presented results are computed with a square inner conductor whose area is the same as that of the circular probe, obtaining results very close to the HFSS simulation. Since the results are very similar to those with 5 steps, the analysis can be carried out very efficiently with the simple square probe. The results for a back to back coaxial to ridge resonator junction are shown in Fig. 9.b.

Finally, another structure which can be modeled by MM is a bifurcation in stripline (or rectangular coaxial), shown in Fig. 10.a. The structure has an inner conductor and an enclosure that vary in order to divide the power into two isolated stripline ports. The response is shown in Fig. 10.b. The structure is also computed exclusively with TEM modes to illustrate the influence of the higher order modes in the response.

5. Conclusions

This chapter has introduced the main concepts of the Mode-Matching (MM) methods for the CAD of waveguide devices. The key idea is to segment the problem under analysis in different waveguide regions where the electromagnetic field is represented by the superposition of modes. At the interface between regions, those modal series have to be matched to fulfill the boundary conditions. This process leads to the Generalized Scattering Matrix (GSM) representation of the problem.

This idea has been applied to the cascading of several transmission systems with different cross-sections. This type of problem could represent many waveguide devices such as filters, transformers, N-furcations, diplexers, polarizers, etc.

Different types of basic discontinuities have been shown, with their corresponding formulations and intrinsic properties for the obtained GSM. Some examples have been introduced in
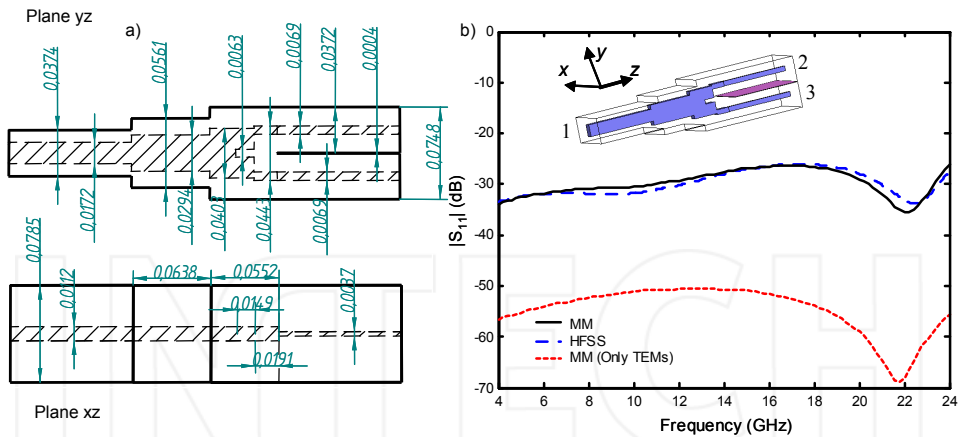
Fig. 10. Configuration of the stripline (rectangular coaxial) bifurcation ($\varepsilon_r = 5.9$). a) Actual aspect ratio and dimensions (inch). b) Return loss at port one.

order to validate the theory with measured experimental data and with the results obtained with other numerical methods.

One important idea to emphasize is the building-block concept, since it provides a simple algorithm to solve more complex problems: the discontinuities are individually characterized and then are cascaded. This idea can be extended to other problems, as long as it is known how to compute the GSM of the building blocks in the structure.

The MM technique has been used for many years and, nowadays, can be considered as an industry standard for some types of problems like the cascading of rectangular or circular waveguides in filters, couplers or horns. Since the formulation of the technique is well known, the latest developments have been oriented towards broadening the range of problems where the method can be applied. The theory shown in this chapter is the basis for more evolved formulations.

A. Appendix. Cylindrical waveguides

The total electromagnetic field in a cylindrical waveguide (see Fig. 11.a) of arbitrary cross section S, with perfect conductivity walls $\sigma = \infty$, filled with isotropic and homogeneous dielectric, can be represented by a modal series as (1) (Collin, 1991).

The homogeneous medium of electric permeability $\varepsilon = \varepsilon_r \varepsilon_0$ and magnetic permeability $\mu = \mu_r \mu_0$ may have losses $\varepsilon_r = \varepsilon'_r - j\varepsilon''_r, \mu_r = \mu'_r - j\mu''_r$, resulting in a complex wavenumber $k = \omega\sqrt{\mu\varepsilon}$ and complex intrinsic impedance of the medium $\eta = \sqrt{\mu/\varepsilon}$. For a lossless waveguide $\varepsilon''_r = \mu''_r = 0$.

The pairs $(\vec{\mathbf{E}}^{\pm}_n, \vec{\mathbf{H}}^{\pm}_n)$, travelling along $\pm z$, respectively, are the electromagnetic fields of a TEM, TE or TM mode[2]: solutions to Maxwell's equations which satisfy the corresponding boundary conditions at the contour C. The modes are not restricted to be propagating; they have at

---

[2] The TEM, TE, TM modes are also called O, H, E, respectively. When it is needed to identify them, the scripts $(o), (h), (e)$ will be used.
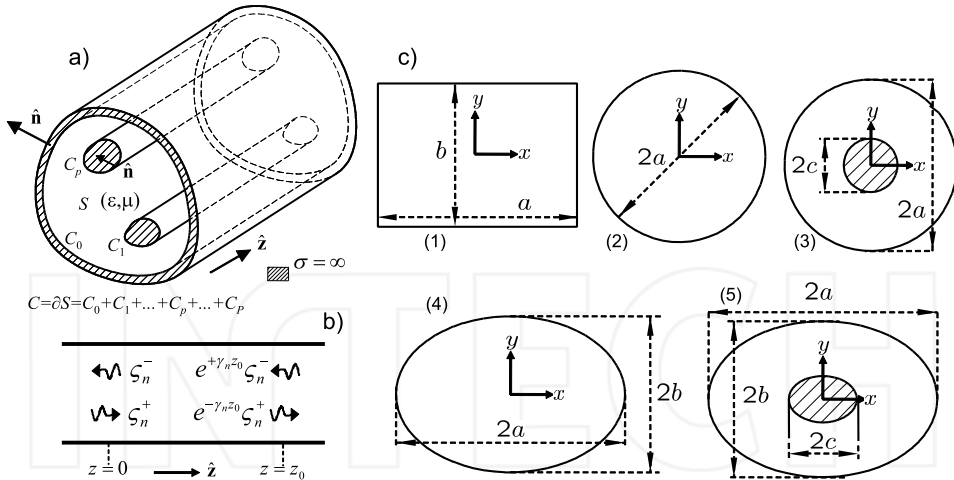
Fig. 11. Multi-conductor cylindrical waveguide closed by perfect conducting walls with homogeneous and isotropic dielectric: a) geometry, b) equivalent transmission line with $\pm\hat{\mathbf{z}}$ modal amplitudes. c) Cross section of some common canonical waveguides: rectangular, circular, circular coaxial, elliptical, confocal elliptical coaxial.

the operating frequency $f = \omega/2\pi$ a complex propagation constant that can be: pure real (evanescent mode), imaginary (propagating mode) or complex with non vanishing real and imaginary part ($\varepsilon_r'' \neq 0$ and/or $\mu_r'' \neq 0$). They are written as:

$$\vec{\mathbf{E}}_n^+ = (\vec{\mathbf{e}}_{tn}^+ + e_{zn}^+\hat{\mathbf{z}})e^{-\gamma_n z} \qquad \vec{\mathbf{E}}_n^- = (\vec{\mathbf{e}}_{tn}^- + e_{zn}^-\hat{\mathbf{z}})e^{+\gamma_n z}$$

$$\vec{\mathbf{H}}_n^+ = (\vec{\mathbf{h}}_{tn}^+ + h_{zn}^+\hat{\mathbf{z}})e^{-\gamma_n z} \qquad \vec{\mathbf{H}}_n^- = (\vec{\mathbf{h}}_{tn}^- + h_{zn}^-\hat{\mathbf{z}})e^{+\gamma_n z}.$$

Since the forward and backward modal solutions are related by simple sign changes, the notation can be simplified:

$$\vec{\mathbf{e}}_n \equiv \vec{\mathbf{e}}_{tn}^+ = \vec{\mathbf{e}}_{tn}^-,\ e_{zn} \equiv e_{zn}^+ = -e_{zn}^-,\ \vec{\mathbf{h}}_n \equiv \vec{\mathbf{h}}_{tn}^+ = -\vec{\mathbf{h}}_{tn}^-,\ h_{zn} \equiv h_{zn}^+ = h_{zn}^-$$

Therefore, (1) is conveniently expressed as:

$$\vec{\mathbf{E}} = \sum_n \left\{ \varsigma_n^+ (\vec{\mathbf{e}}_n + e_{zn}\hat{\mathbf{z}})e^{-\gamma_n z} + \varsigma_n^- (+\vec{\mathbf{e}}_n - e_{zn}\hat{\mathbf{z}})e^{+\gamma_n z} \right\} \tag{30a}$$

$$\vec{\mathbf{H}} = \sum_n \left\{ \varsigma_n^+ (\vec{\mathbf{h}}_n + h_{zn}\hat{\mathbf{z}})e^{-\gamma_n z} + \varsigma_n^- (-\vec{\mathbf{h}}_n + h_{zn}\hat{\mathbf{z}})e^{+\gamma_n z} \right\}. \tag{30b}$$

The terms $\varsigma_n^\pm e^{\mp\gamma_n z}$ are called the modal amplitudes at an arbitrary plane z. Thus, $\varsigma_n^\pm$ are the modal amplitudes at $z = 0$ (see Fig. 11.b). The vector functions $\vec{\mathbf{e}}_n, \vec{\mathbf{h}}_n$, and the scalars functions e_{zn}, h_{zn} exclusively depend on the transversal coordinates and $\vec{\mathbf{e}}_n, \vec{\mathbf{h}}_n$ are perpendicular to $\hat{\mathbf{z}}$. They are related by the modal wave impedance/admittance:

$$\vec{\mathbf{e}}_n = Z_n \vec{\mathbf{h}}_n \times \hat{\mathbf{z}}, \quad \vec{\mathbf{h}}_n = Y_n \hat{\mathbf{z}} \times \vec{\mathbf{e}}_n, \quad Z_n = Y_n^{-1}. \tag{31}$$

The formal expressions for the modal fields of any waveguide as in Fig. 11.a are given now. Later, the mode normalization used in the chapter and the specific solutions for the canonical waveguides in Fig. 11.c are introduced.

A.1 TEM modes (*o*-modes)

In a structure with $P + 1$ conductors (each one with contour C_p), P linearly independent TEM (*Transversal ElectroMagnetic*) modes must be included in the modal series ($P \geq 0$). They are solution to the Laplace equation with non-homogeneous Dirichlet boundary conditions:

$$\triangle_t \Phi_n = 0, \quad \Phi_n \big|_{C_p} = v_{np}, \quad p = 0, \ldots, P, \quad n = 1, \ldots, P. \tag{32}$$

The electromagnetic field[3] is given by:

$$\vec{e}_n = Q_n^{\frac{1}{2}} Z_n^{\frac{1}{2}} \vec{\Phi}_{En} = Q_n^{\frac{1}{2}} Z_n^{\frac{1}{2}} \nabla_t \Phi_n, \qquad e_{zn} = 0$$
$$\vec{h}_n = Q_n^{\frac{1}{2}} Y_n^{\frac{1}{2}} \vec{\Phi}_{Hn} = Q_n^{\frac{1}{2}} Y_n^{\frac{1}{2}} \hat{\mathbf{z}} \times \nabla_t \Phi_n, \quad h_{zn} = 0. \tag{33}$$

where Q_n is an arbitrary normalization constant and $\vec{\Phi}_{En}, \vec{\Phi}_{Hn}$ are obtained from Φ_n by simple gradient operations. The propagation constant and wave impedance for all the TEM modes are:

$$\gamma_n = j\omega\sqrt{\mu\varepsilon} = jk, \quad Z_n = Y_n^{-1} = \sqrt{\frac{\mu}{\varepsilon}} = \eta. \tag{34}$$

A.2 TE modes (*h*-modes)

The electromagnetic field of a TE (*Transversal Electric*) mode is obtained by solving the Helmholtz equation with homogeneous Neumann boundary conditions:

$$\triangle_t \Phi_n + k_{cn}^2 \Phi_n = 0, \quad (\nabla_t \Phi_n \cdot \hat{\mathbf{n}})\big|_C = 0, \quad \iint_S |\nabla_t \Phi_n|^2 dS = k_{cn}^2 \iint_S \Phi_n^2 dS = 1. \tag{35}$$

The field, with arbitrary normalization constant Q_n, is expressed as:

$$\vec{e}_n = Q_n^{\frac{1}{2}} Z_n^{\frac{1}{2}} \vec{\Phi}_{En} = Q_n^{\frac{1}{2}} Z_n^{\frac{1}{2}} \nabla_t \Phi_n \times \hat{\mathbf{z}}, \quad e_{zn} = 0$$
$$\vec{h}_n = Q_n^{\frac{1}{2}} Y_n^{\frac{1}{2}} \vec{\Phi}_{Hn} = Q_n^{\frac{1}{2}} Y_n^{\frac{1}{2}} \nabla_t \Phi_n, \qquad h_{zn} = -Q_n^{\frac{1}{2}} Y_{\omega n}^{\frac{1}{2}} \frac{k_{cn}^2}{\gamma_n} \Phi_n, \tag{36}$$

where the propagation constant and wave impedance are given by:

$$\gamma_n = \sqrt{k_{cn}^2 - \omega^2\mu\varepsilon} = \sqrt{k_{cn}^2 - k^2}, \quad Z_n = Y_n^{-1} = \frac{j\omega\mu}{\gamma_n} = \frac{jk\eta}{\gamma_n}. \tag{37}$$

A.3 TM modes (*e*-modes)

The electromagnetic field of a TM (*Transversal Magnetic*) mode is obtained by solving the Helmholtz equation with homogeneous Dirichlet boundary conditions

$$\triangle_t \Phi_n + k_{cn}^2 \Phi_n = 0, \quad \Phi_n\big|_C = 0, \quad \iint_S |\nabla_t \Phi_n|^2 dS = k_{cn}^2 \iint_S \Phi_n^2 dS = 1. \tag{38}$$

---

[3] For maintaining a formal similarity with a TM mode with $k_{cn} = 0$, the electric field is calculated as $\nabla_t \Phi_n$ and not as $-\nabla_t \Phi_n$. Therefore, v_{np} is the opposite of the electrostatic voltage.

The field, with arbitrary normalization constant Q_n, is expressed as:

$$
\begin{aligned}
\vec{\mathbf{e}}_n &= Q_n^{\frac{1}{2}} Z_n^{\frac{1}{2}} \vec{\boldsymbol{\Phi}}_{En} = Q_n^{\frac{1}{2}} Z_n^{\frac{1}{2}} \nabla_t \Phi_n, & e_{zn} &= -Q_n^{\frac{1}{2}} Z_n^{\frac{1}{2}} \frac{k_{cn}^2}{\gamma_n} \Phi_n \\
\vec{\mathbf{h}}_n &= Q_n^{\frac{1}{2}} Y_n^{\frac{1}{2}} \vec{\boldsymbol{\Phi}}_{Hn} = Q_n^{\frac{1}{2}} Y_n^{\frac{1}{2}} \hat{\mathbf{z}} \times \nabla_t \Phi_n, & h_{zn} &= 0
\end{aligned}
\tag{39}
$$

where the propagation constant and wave impedance are given by[4]:

$$
\gamma_n = \sqrt{k_{cn}^2 - \omega^2 \mu \varepsilon} = \sqrt{k_{cn}^2 - k^2}, \quad Z_n = Y_n^{-1} = \frac{\gamma_n}{j\omega\varepsilon} = \frac{\gamma_n \eta}{jk}.
\tag{40}
$$

A.4 Mode orthogonality and normalization

A very useful property of the modes is the orthogonality:

$$
\iint_S \vec{\mathbf{e}}_m \times \vec{\mathbf{h}}_n \cdot \hat{\mathbf{z}}\, dS = Y_n \iint_S \vec{\mathbf{e}}_m \cdot \vec{\mathbf{e}}_n\, dS = Z_m \iint_S \vec{\mathbf{h}}_m \cdot \vec{\mathbf{h}}_n\, dS = Q_n \delta_{mn},
\tag{41}
$$

In (Collin, 1991), this relation is shown for modes with different cutoff wave number (non degenerate). In any other case, an orthogonalization process may be carried out. Thus, in this chapter is used a set of modes (33),(36),(39) where (41) always holds.

It is stressed that the Φ solutions (32),(35),(38) and their related vectors $\vec{\boldsymbol{\Phi}}_E, \vec{\boldsymbol{\Phi}}_H$ do not depend on the waveguide dielectric and can be written as frequency independent functions that take real values. Q_n is a complex normalization factor that may vary with frequency and can be arbitrarily chosen (for instance it is common to set $Q_n = 1$).

Another important orthogonality relation is

$$
\iint_S \vec{\mathbf{e}}_m \times \vec{\mathbf{h}}_n^* \cdot \hat{\mathbf{z}}\, dS = Y_n^* \iint_S \vec{\mathbf{e}}_m \cdot \vec{\mathbf{e}}_n^*\, dS = Z_m \iint_S \vec{\mathbf{h}}_m \cdot \vec{\mathbf{h}}_n^*\, dS = P_n \delta_{mn},
\tag{42}
$$

which is related to (41) by:

$$
P_n = \frac{\sqrt{Z_n}}{(\sqrt{Z_n})^*} |Q_n| \overset{\varepsilon_r'' = \mu_r'' = 0}{=}
\begin{cases}
|Q_n| & n\ prop. & (k \geq k_{cn}) \\
+j|Q_n| & n\ evan.\ TE & (k < k_{cn}) \\
-j|Q_n| & n\ evan.\ TM & (k < k_{cn})
\end{cases}.
\tag{43}
$$

Once Q_n is fixed, P_n cannot be independently defined. Moreover, for a lossless waveguide, at frequencies where $k \geq k_{cn}$ (propagating mode, operating frequency above the cutoff frequency $f \geq f_{cn} = k_{cn}/(2\pi\sqrt{\mu\varepsilon})$), γ_n is pure imaginary and Z_n is real. For $k < k_{cn}$ (*evanescent* mode, $f < f_{cn}$), γ_n is real and Z_n is pure imaginary. In terms of complex power flow, as (43) shows, P_n is real for propagating modes and imaginary for evanescent modes.

A.5 Canonical waveguides

There are several waveguide cross sections that allow analytical TEM, TE and TM solutions, as circular or coaxial sectors (elliptical sectors as well), contours described in parabolic coordinates or 30, 45 and 60 degrees triangles. The more common are the following, using standard rectangular, circular and elliptical coordinates.

---

[4] The TEM eqs. (33),(34) can be formally considered as a particular case of (39),(40) with $k_{cn} = 0$.

A.5.1 Rectangular waveguide

Regarding Fig. 11.c1, where the reference system is placed at the rectangular cross section center, the TE and TM solutions to (35),(38) are $((m,n) \neq (0,0))$:

$$
\begin{aligned}
(H_{mn})\, \Phi_{mn}^{(h)} &= (N_{mn}^{(h)})^{\frac{1}{2}} \cos\left(\tfrac{m\pi}{a}(x+\tfrac{a}{2})\right) \cos\left(\tfrac{n\pi}{b}(y+\tfrac{b}{2})\right), \ m,n = 0,1,\dots \\
(E_{mn})\, \Phi_{mn}^{(e)} &= (N_{mn}^{(e)})^{\frac{1}{2}} \sin\left(\tfrac{m\pi}{a}(x+\tfrac{a}{2})\right) \sin\left(\tfrac{n\pi}{b}(y+\tfrac{b}{2})\right), \ m,n = 1,2,\dots
\end{aligned}
\tag{44}
$$

with cutoff wavenumber and normalization constants ($\epsilon_{mk} = 2\,(m=k), 1\,(m \neq k)$):

$$
k_{c,mn}^{(h)} = \sqrt{(\tfrac{m\pi}{a})^2 + (\tfrac{n\pi}{b})^2}, \quad N_{mn}^{(h)} = \left| \left((\tfrac{m\pi}{a})^2 + (\tfrac{n\pi}{b})^2\right) \tfrac{ab}{4} \epsilon_{m0}\epsilon_{n0} \right|^{-1}.
$$

A.5.2 Circular waveguide

Regarding Fig. 11.c2, the TE and TM solutions to (35),(38) are:

$$
\begin{aligned}
(Hc_{pr})\ \Phi_{pr}^{(hc)} \\
(Hs_{pr})\ \Phi_{pr}^{(hs)}
\end{aligned}
= (N_{pr}^{(h)})^{\frac{1}{2}} \mathrm{J}_p(\tfrac{\xi'_{pr}}{a}\rho) \begin{matrix}\cos \\ \sin\end{matrix}(p\varphi), \quad
p = \begin{matrix}0,1,\dots \\ 1,2,\dots\end{matrix}\ r = 1,2,\dots
\tag{45}
$$

$$
\begin{aligned}
(Ec_{pr})\ \Phi_{pr}^{(ec)} \\
(Es_{pr})\ \Phi_{pr}^{(es)}
\end{aligned}
= (N_{pr}^{(e)})^{\frac{1}{2}} \mathrm{J}_p(\tfrac{\xi_{pr}}{a}\rho) \begin{matrix}\cos \\ \sin\end{matrix}(p\varphi), \quad
p = \begin{matrix}0,1,\dots \\ 1,2,\dots\end{matrix}\ r = 1,2,\dots
$$

with roots (Abramowitz & Stegun, 1956) and normalization constants:

$$
\begin{aligned}
k_{c,pr}^{(h)} &= \tfrac{\xi'_{pr}}{a}, \ \mathrm{J}'_p(\xi'_{pr}) = 0, \ N_{pr}^{(h)} = |\epsilon_{p0}\tfrac{\pi}{2}(\xi'^2_{pr} - p^2)\mathrm{J}_p^2(\xi'_{pr})|^{-1} \\
k_{c,pr}^{(e)} &= \tfrac{\xi_{pr}}{a}, \ \mathrm{J}_p(\xi_{pr}) = 0, \ N_{pr}^{(e)} = |\epsilon_{p0}\tfrac{\pi}{2}\xi_{pr}^2 \mathrm{J}_p'^2(\xi_{pr})|^{-1}.
\end{aligned}
\tag{46}
$$

A.5.3 Circular coaxial waveguide

The TEM mode corresponding to (33) in a circular coaxial waveguide (Fig. 11.c3) of inner radius c and outer radius a is

$$
\Phi^{(o)} = (N^{(o)})^{\frac{1}{2}} \ln\tfrac{\rho}{a}, \quad N^{(o)} = \left|2\pi \ln\tfrac{a}{c}\right|^{-1}, \quad Z_c = \tfrac{\eta}{2\pi}\ln\tfrac{a}{c}.
\tag{47}
$$

The TE and TM solutions to (35),(38) are:

$$
\begin{aligned}
(Hc_{pr})\ \Phi_{pr}^{(hc)} \\
(Hs_{pr})\ \Phi_{pr}^{(hs)}
\end{aligned}
= (N_{pr}^{(h)})^{\frac{1}{2}} R_p^{(h)}(\tfrac{\xi'_{pr}}{a}\rho) \begin{matrix}\cos \\ \sin\end{matrix}(p\varphi), \quad
p = \begin{matrix}0,1,\dots \\ 1,2,\dots\end{matrix}\ r = 1,2,\dots
\tag{48}
$$

$$
\begin{aligned}
(Ec_{pr})\ \Phi_{pr}^{(ec)} \\
(Es_{pr})\ \Phi_{pr}^{(es)}
\end{aligned}
= (N_{pr}^{(e)})^{\frac{1}{2}} R_p^{(e)}(\tfrac{\xi_{pr}}{a}\rho) \begin{matrix}\cos \\ \sin\end{matrix}(p\varphi), \quad
p = \begin{matrix}0,1,\dots \\ 1,2,\dots\end{matrix}\ r = 1,2,\dots,
$$

where the radial functions with their roots (Abramowitz & Stegun, 1956) are:

$$
\begin{aligned}
R_p^{(h)}(u) &= \mathrm{Y}'_p(\xi'_{pr})\mathrm{J}_p(u) - \mathrm{J}'_p(\xi'_{pr})\mathrm{Y}_p(u), \quad R_p'^{(h)}(\xi'_{pr}\tfrac{c}{a}) = 0, \quad k_{c,pr}^{(h)} = \tfrac{\xi'_{pr}}{a} \\
R_p^{(e)}(u) &= \mathrm{Y}_p(\xi_{pr})\mathrm{J}_p(u) - \mathrm{J}_p(\xi_{pr})\mathrm{Y}_p(u), \quad R_p^{(e)}(\xi_{pr}\tfrac{c}{a}) = 0, \quad k_{c,pr}^{(e)} = \tfrac{\xi_{pr}}{a}.
\end{aligned}
\tag{49}
$$

The normalization constants are

$$
\begin{aligned}
N_{pr}^{(h)} &= |\epsilon_{p0}\tfrac{\pi}{2}((\xi'^2_{pr} - p^2)R_{pr}^{(h)2}(\xi'_{pr}) - ((\xi'_{pr}\tfrac{c}{a})^2 - p^2)R_{pr}^{(h)2}(\xi'_{pr}\tfrac{c}{a}))|^{-1} \\
N_{pr}^{(e)} &= |\epsilon_{p0}\tfrac{\pi}{2}(\xi_{pr}^2 R_{pr}^{(e)'2}(\xi_{pr}) - (\xi_{pr}\tfrac{c}{a})^2 R_{pr}^{(e)'2}(\xi_{pr}\tfrac{c}{a}))|^{-1}.
\end{aligned}
\tag{50}
$$

A.5.4 Elliptical and confocal elliptical coaxial waveguides

An elliptic contour (Fig. 11.c4) of axes $2a, 2b$ is described in elliptic coordinates

$$x = d_f \cosh \varrho \cos \vartheta, \quad y = d_f \sinh \varrho \sin \vartheta, \quad \varrho \geq 0, -\pi \leq \vartheta < \pi,$$

as $\varrho = \varrho_a = \mathrm{acosh}\, a/d_f$, where $d_f{}^2 = a^2 - b^2$ is half the focal distance. A second confocal ellipse with major axis $2c$ (Fig. 11.c5) is described by $\varrho = \varrho_c = \mathrm{acosh}\, c/d_f$.

The solutions to the Helmholtz equation in elliptic coordinates is written as $\Phi = R(\varrho)a(\vartheta)$, a and R being solutions to the Mathieu and modified Mathieu equation, respectively, with parameter q_0 (Mclachlan, 1964). With them, the TE and TM modes (35),(38) of the elliptical waveguide are classified as follows:

$$
\begin{aligned}
(Hc_{pr}) \; \Phi_{pr}^{(hc)} &= (N_{pr}^{(hc)})^{\frac{1}{2}} R_p^{(hc)}(\varrho, q'_{cpr}) \, \mathrm{ce}_p(\vartheta, q'_{cpr}), \; p = 0,1,\ldots; r = 1,2,\ldots \\
(Hs_{pr}) \; \Phi_{pr}^{(hs)} &= (N_{pr}^{(hs)})^{\frac{1}{2}} R_p^{(hs)}(\varrho, q'_{spr}) \, \mathrm{se}_p(\vartheta, q'_{spr}), \; p = 1,2,\ldots; r = 1,2,\ldots \\
(Ec_{pr}) \; \Phi_{pr}^{(ec)} &= (N_{pr}^{(ec)})^{\frac{1}{2}} R_p^{(ec)}(\varrho, q_{cpr}) \, \mathrm{ce}_p(\vartheta, q_{cpr}), \; p = 0,1,\ldots; r = 1,2,\ldots \\
(Es_{pr}) \; \Phi_{pr}^{(es)} &= (N_{pr}^{(es)})^{\frac{1}{2}} R_p^{(es)}(\varrho, q_{spr}) \, \mathrm{se}_p(\vartheta, q_{spr}), \; p = 1,2,\ldots; r = 1,2,\ldots
\end{aligned}
\tag{51}
$$

Referring to both waveguides (although their radial functions are different), the roots and cutoff wavenumbers are (Alhargan & Judah, 1994), (Alhargan & Judah, 1996):

$$
\begin{aligned}
R_p'^{(hc)}(\varrho_a, q'_{cpr}) = 0, \; R_p^{(ec)}(\varrho_a, q_{cpr}) = 0 \\
R_p'^{(hs)}(\varrho_a, q'_{spr}) = 0, \; R_p^{(es)}(\varrho_a, q_{spr}) = 0
\end{aligned}
\;, \quad k_c = \frac{2}{d_f}\sqrt{q_0} = \frac{2}{a}\sqrt{q_0}\cosh\varrho_a,
$$

The normalization constants are:

$$N^{\binom{h}{e}} = |2\pi q_0 \int_{\varrho_0}^{\varrho_a} R^2(\varrho)(\cosh 2\varrho - I^{\binom{h}{e}})d\varrho|^{-1}, \; I^{\binom{h}{e}} = \frac{1}{\pi}\int_{-\pi}^{\pi} a^2(\vartheta)\cos 2\vartheta\, d\vartheta, \tag{52}$$

with $\varrho_0 = 0$ for the elliptical waveguide and $\varrho_0 = \varrho_c$ for the coaxial waveguide. The angular integral can be done analytically. Then, the radial integral is computed numerically. The TEM solution (33) for the confocal elliptical coaxial waveguide is:

$$\phi^{(o)} = (N^{(o)})^{\frac{1}{2}}(\varrho - \varrho_a), \; N^{(o)} = |2\pi(\varrho_a - \varrho_c)|^{-1}, \; Z_c = \frac{\eta}{2\pi}\ln\frac{a+\sqrt{a^2-d_f^2}}{c+\sqrt{c^2-d_f^2}}. \tag{53}$$

B. References

Abramowitz, M. & Stegun, I. (1956). *Handbook of Mathematical Functions*, Dover Publications Inc., New York.

Alhargan, F. & Judah, S. (1994). Tables of normalized cutoff wavenumbers of elliptic cross section resonators, *IEEE Trans. Microw. Theory Tech.* **42**(2): 333–338.

Alhargan, F. & Judah, S. (1996). Mode charts for confocal annular elliptic resonators, *IEE Proc. Microw., Antennas and Propagat.* **143**(4): 358–360.

Bozzi, M., Conciauro, G. & Perregrini, L. (2002). On the evaluation of modal coupling coefficients by contour integrals, *IEEE Trans. Microw. Theory Tech.* **50**(7): 1853–1855.

Chan, K.-L. & Judah, S. (1997). Two port scattering at an elliptical-waveguide junction, *IEEE Trans. Microw. Theory Tech.* **45**(8): 1255–1262.

Clarricoats, P. J. B. & Slinn, K. R. (1966). Numerical method for the solution of waveguide discontinuity problems, *Electronic Letters* pp. 226–227.

Collin, R. E. (1991). *Field Theory of Guided Waves*, IEEE Press, New York.

Conciauro, G., Guglielmi, M. & Sorrentino, R. (1999). *Advanced modal analysis: CAD techniques for waveguide components and filters*, John Wiley.

Drabuwitch, S. W. (1966). Multimode antennas, *Microwave Journal* **9**: 41–51.

Figlia, G. & Gentili, G. G. (2002). On the line-integral formulation of Mode-Matching technique, *IEEE Trans. Microw. Theory Tech.* **50**: 578–580.

Gentili, G. G. (1991). Properties of TE-TM Mode-Matching techniques, *IEEE Trans. Microw. Theory Tech.* **39**(9): 1669–1673.

Gerini, G. & Guglielmi, M. (2001). Full-wave CAD of a rectangular waveguide filter with integrated coaxial excitation, *IEEE Trans. Microw. Theory Tech.* **49**: 986–990.

Haskal, H. (1964). Matrix description of waveguide discontinuities in the presence of evanescent modes, *IEEE Trans. Microw. Theory Tech.* pp. 184–188.

Itoh (editor), T. (1989). *Numerical Techniques for Microwave and Millimeter-Wave Passive-Structures*, John Wiley, New York.

Leroy, M. (1983). On the convergence of numerical results in Modal Analysis, *IEEE Trans. Antennas Propagat.* **31**(4): 655–659.

MacPhie, R. H. & Wu, K. L. (1995). Scattering at the junction of a rectangular waveguide and a larger circular waveguide, *IEEE Trans. Microw. Theory Tech.* **43**(9): 2041–2045.

Mclachlan, N. (1964). *Theory and application of Mathieu functions*, Dover Pub., New York.

Mittra, R. & Lee, W. W. (1971). *Analytical techniques in the theory of guided waves*, MacMillan, New York.

Mongiardo, M. & Tomassoni, C. (2000). Modal analysis of discontinuities between elliptical waveguides, *IEEE Trans. Microw. Theory Tech.* **48**(4): 597–605.

Omar, A., Eleftheriades, G. & Katehi, L. (1994). Some important properties of waveguide junction generalized scattering matrices in the context of the mode matching technique, *IEEE Trans. Microw. Theory Tech.* **42**(10): 1896–1903.

Orfanidis, A., Kyriacou, G. & Sahalos, J. (2000). A mode-matching technique for the study of circular and coaxial waveguide discontinuities based on closed-form coupling integrals, *IEEE Trans. Microw. Theory Tech.* **48**(5): 880–883.

Patzelt, H. & Arndt, F. (1982). Double-plane steps in rectangular waveguides and their application for transformers, irises, and filters, *IEEE Trans. Microw. Theory Tech.* **82**(5): 771–776.

Ruiz-Cruz, J. A., Montejo-Garai, J. R. & Rebollar, J. M. (2002). Characterisation of waveguide discontinuities with finite wall conductivity, *Proc. 2002 IEEE Antennas and Propagation Symp. Dig., Columbus, OH* **4**: 428–431.

Ruiz-Cruz, J. A., Zaki, K. A. & Rebollar, J. M. (2004). Mode-matching analysis of a coaxial-to-stripline discontinuity applied to the modelling of a coaxial probe, *Proc. 2004 IEEE Antennas and Propagation Symp. Dig., Monterey, CA* **2**: 2139–2142.

Senior, T. B. A. (1960). Impedance boundary conditions for imperfectly conducting surfaces, *Applied Science Research, section B* **8**: 418–436.

Shen, Z. X. & MacPhie, R. H. (1990). Conservation of complex power technique for waveguide junctions with finite wall conductivity, *IEEE Trans. Microw. Theory Tech.* **38**(4): 373–378.

Uher, J., Bornemann, J. & Rosenberg, U. (1993). *Waveguide Components for Antenna Feed Systems*, Artech House, Boston.

Vassallo, C. (1985). *Thorie des guides d'ondes lectromagntiques*, Collection Technique et Scientifique des Telcommunications (CNET), Eyrolles, Paris.

Wexler, A. (1967). Solution of waveguides discontinuities by modal analysis, *IEEE Transactions on Microwave Theory and Techniques* **15**: 508–517.

Zhongxiang, S. & MacPhie, R. H. (1995). Scattering by a thick off-centered circular iris in circular waveguide, *IEEE Trans. Microw. Theory Tech.* **43**(11): 2639–2642.
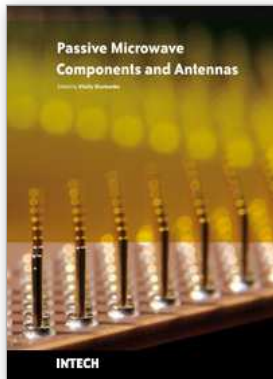
Passive Microwave Components and Antennas

Edited by Vitaliy Zhurbenko

Modelling and computations in electromagnetics is a quite fast-growing research area. The recent interest in this field is caused by the increased demand for designing complex microwave components, modeling electromagnetic materials, and rapid increase in computational power for calculation of complex electromagnetic problems. The first part of this book is devoted to the advances in the analysis techniques such as method of moments, finite-difference time- domain method, boundary perturbation theory, Fourier analysis, mode-matching method, and analysis based on circuit theory. These techniques are considered with regard to several challenging technological applications such as those related to electrically large devices, scattering in layered structures, photonic crystals, and artificial materials. The second part of the book deals with waveguides, transmission lines and transitions. This includes microstrip lines (MSL), slot waveguides, substrate integrated waveguides (SIW), vertical transmission lines in multilayer media as well as MSL to SIW and MSL to slot line transitions.

How to reference

In order to correctly reference this scholarly work, feel free to copy and paste the following:

Jorge A. Ruiz-Cruz, Jose R. Montejo-Garai and Jesus M. Rebollar (2010). Computer Aided Design of Waveguide Devices by Mode-Matching Methods, Passive Microwave Components and Antennas, Vitaliy Zhurbenko (Ed.), ISBN: 978-953-307-083-4, InTech, Available from: http://www.intechopen.com/books/passive-microwave-components-and-antennas/computer-aided-design-of-waveguide-devices-by-mode-matching-methods

INTECH
open science | open minds